


ORIGINAL ARTICLE

New cellular imaging-based method to distinguish the SPG4 subtype of hereditary spastic paraplegia

Francesca Sardina¹  | Davide Valente^{1,2} | Gaia Fattorini^{1,3} | Ettore Cioffi⁴ | Gianmarco Dalla Zanna⁴ | Alessandra Tessa⁵ | Daniela Trisciuglio¹ | Silvia Soddu² | Filippo M. Santorelli⁵ | Carlo Casali⁴ | Cinzia Rinaldo¹

¹Institute of Molecular Biology and Pathology (IBPM), Consiglio Nazionale delle Ricerche (CNR), c/o Sapienza University of Rome, Rome, Italy

²Unit of Cellular Networks and Molecular Therapeutic Targets, IRCCS-Regina Elena National Cancer Institute, Rome, Italy

³Department of Biology and Biotechnology, "Charles Darwin" Sapienza University of Rome, Rome, Italy

⁴Department of Medico-Surgical Sciences and Biotechnologies, Sapienza University of Rome, Latina, Italy

⁵Molecular Medicine, IRCCS Fondazione Stella Maris, Pisa, Italy

Correspondence

Francesca Sardina, Institute of Molecular Biology and Pathology (IBPM), Consiglio Nazionale delle Ricerche (CNR), c/o Sapienza University of Rome, Rome, Italy.
Email: francesca.sardina3@gmail.com

Funding information

AFM-Telethon, Grant/Award Number: 22157 and 23786; AIViPS; Euro-HSP; Fondazione Telethon; Ministero della Salute; Regione Lazio; UK-HSP-support

Abstract

Background and purpose: Microtubule defects are a common feature in several neurodegenerative disorders, including hereditary spastic paraplegia. The most frequent form of hereditary spastic paraplegia is caused by mutations in the *SPG4/SPAST* gene, encoding the microtubule severing enzyme spastin. To date, there is no effective therapy available but spastin-enhancing therapeutic approaches are emerging; thus prognostic and predictive biomarkers are urgently required.

Methods: An automated, simple, fast and non-invasive cell imaging-based method was developed to quantify microtubule cytoskeleton organization changes in lymphoblastoid cells and peripheral blood mononuclear cells.

Results: It was observed that lymphoblastoid cells and peripheral blood mononuclear cells from individuals affected by *SPG4*-hereditary spastic paraplegia show a polarized microtubule cytoskeleton organization. In a pilot study on freshly isolated peripheral blood mononuclear cells, our method discriminates *SPG4*-hereditary spastic paraplegia from healthy donors and other hereditary spastic paraplegia subtypes. In addition, it is shown that our method can detect the effects of spastin protein level changes.

Conclusions: These findings open the possibility of a rapid, non-invasive, inexpensive test useful to recognize *SPG4*-hereditary spastic paraplegia subtype and evaluate the effects of spastin-enhancing drug in non-neuronal cells.

KEYWORDS

biomarker, hereditary spastic paraplegia, microtubule, SPG4

INTRODUCTION

Hereditary spastic paraplegia (HSP) is a genetic motoneuron disease characterized by lower limb spasticity resulting from slowly progressive degeneration of long corticospinal axons [1]. Thus far, more than 85 distinct spastic paraplegia genes (*SPG*) have been identified.

Proteins encoded by the *SPG* genes have diverse functions in several interrelated cellular pathways, such as microtubule (MT) dynamics, intracellular trafficking, mitochondrial functions, fatty acid and phospholipid metabolism, endoplasmic reticulum shaping and stress response, and autophagy [2]. Mutations in the *SPG4/SPAST* gene account for 40%–60% of autosomal dominant HSPs with about 86%

This is an open access article under the terms of the [Creative Commons Attribution-NonCommercial-NoDerivs](https://creativecommons.org/licenses/by-nc-nd/4.0/) License, which permits use and distribution in any medium, provided the original work is properly cited, the use is non-commercial and no modifications or adaptations are made.

© 2023 The Authors. *European Journal of Neurology* published by John Wiley & Sons Ltd on behalf of European Academy of Neurology.

penetrance and 20% of sporadic patients [3]. Spastin is an MT severing enzyme encoded by the *SPG4* gene, which produces two spastin isoforms called M1 (68 kDa) and M87 (60 kDa) by two different initiation codons. M87 is the predominant form in all tissues, whereas M1 is only detectable in neuronal tissues [4]. M1 and M87 have alternative splicing variants, lacking the exon 4 [4]. More than 250 mutations of the *SPG4* gene have been reported, which can be subdivided into missense mutations (inactivating mutations clustering mainly in the catalytic domain and other mutations whose functional outcome is largely unknown) and into truncating mutations (frameshift, nonsense and insertions/deletions, commonly associated with a reduced amount of spastin protein as a result of mRNA nonsense-mediated decay) [5]. Therefore, *SPG4*-HSP is mostly thought to be mediated by haploinsufficiency and insufficient MT severing activity [1]. For a given variant, age at onset, clinical severity and course of progression are highly variable and unpredictable, even in the same family [3,5-7]. To predict the probability of fast disease progression, fluid biomarkers are emerging. The concentration of neurofilament light in cerebrospinal fluid or in serum appears a promising prognostic tool in the prodromal phase of *SPG4*-HSP and in young *SPG4*-HSP patients [8-11].

To date, no effective disease-modifying therapies are currently available, but approaches based on drugs counteracting dysfunctional mechanisms or spastin-enhancing treatments are emerging [7]. A gene-dosage rescue of neurite defects has been reported in neurons from *SPG4*-HSP patients, showing that restoring physiological spastin levels might halt pathological phenotypes [12].

Recently, it was demonstrated that spastin stability is regulated by the ubiquitin-proteasome system in a neddylation-dependent manner and it was shown that the inhibition of its poly-ubiquitylation, using the neddylation inhibitor MLN4924, increases spastin protein levels and rescues neurite defects in spastin-deficient models [13]. No predictive biomarker able to determine which patients are likely to respond to therapy is available.

Spastin regulates cytoskeleton rearrangement associated with membrane and MT remodelling and dynamics [14, 15]. MTs play a key role in maintaining cell morphology and motility. In neurons, MT dynamics promote axon growth, maintenance and trafficking. Spastin is a critical player in cytokinesis and nuclear envelope resealing during cell division, in intracellular traffic of different cell types and in axonal transport of neurons [16]. Recently, during studies on spastin regulatory pathways, a polarized MT cytoskeleton organization in lymphoblastoid cells (LCLs) deriving from *SPG4*-HSP patients was observed. Based on these observations, a non-invasive, cell imaging-based method was developed able to discriminate *SPG4*-HSP from healthy donors and other HSP subtypes and to monitor the effects of spastin-enhancing drugs.

METHODS AND MATERIALS

Ethics statement and genotype of the HSP cells

The ethics committee of Asl Roma 2, Rome, Italy, approved this study on patient derived cells (0074975/2020). Written informed consent

was obtained and data analysis was performed anonymously. The HSP genotypes of the patients are reported in Table 1.

Cells and treatments

Mouse motor neuronal NSC-34 cells (a gift of M. Cozzolino) were cultured in Dulbecco's modified Eagle's medium Nutrient Mixture F12 (DMEM-F12) 1:1, supplemented with 10% heat-inactivated foetal bovine serum (FBS). *SPG4* LCLs and healthy donor (HD) LCLs were established by Epstein-Barr virus infection. The LCLs from patients with ataxia-telangiectasia (AT) or Werner syndrome (WS) used in this study have been described previously [17]. Peripheral blood mononuclear cells (PBMCs) were isolated from blood samples in an ethylenediaminetetraacetic acid (EDTA) tube by Lympholyte-H (Cedarlane) density gradient centrifugation, as in Prodosmo et al. [17]. PBMCs and LCLs were cultured in RPMI GlutaMAX (Gibco) supplemented with 10% FBS and were routinely tested for mycoplasma contamination. To perform our analyses on proliferating cells, freshly isolated PBMCs were induced to enter the cell cycle by incubation with 5 µg/ml phytohaemagglutinin (ThermoFisher, 10576015) for 60h.

The following chemicals were used: MLN4924 0.1 µM for 16h (Cayman Chemical 15217), spastazoline 10 µM for 16h (HY-111548, MedChemExpress), valproic acid (VPA) 1mM for 24h (Cayman Chemical 13033) and dimethyl sulfoxide (DMSO) (Sigma-Aldrich).

RNA interference (RNAi)

Spastin RNAi was obtained by using specific short interfering RNAs (siRNAs) selected amongst targeting sequences common to all spastin isoforms, as in Pisciotani et al. [18]. siRNAs were transfected using Amaxa Nucleofector 4D according to the manufacturer's instructions.

Western blot (WB)

Total cell extracts were prepared in RIPA buffer (50mM Tris-HCl pH 8, 150mM NaCl, 0.5% sodium deoxycholate, 0.1% sodium dodecyl sulfate [SDS], 1% NP40 and 1mM EDTA) supplemented with protease and phosphatase inhibitors (Roche). Proteins were resolved by SDS polyacrylamide gel electrophoresis using Bolt Novex Bis-Tris Gels 4%-12% gradient (Life Technologies). Immunoreactivity was determined using ECL Prime (Amersham); image acquisition and densitometry analysis was performed with Image Lab software (Bio-Rad). The following antibodies (Abs) were employed: anti-GAPDH #sc-32233 (1:1000; Santa Cruz Technologies), anti-spastin sp3G11/1 #sc-53443 (1:200; Santa Cruz Technologies), anti-Nedd8 #ab81264 (1:500 Abcam), anti-acetyl- α -tubulin #T7451 (1:1000; Sigma-Aldrich), anti-mouse-HRP #7076 and anti-rabbit-HRP #7074 (Cell Signaling Technology).

TABLE 1 HD and patient cells

HD	Patients		HSP genomic mutation	LCLs	PBMcs
	LCLs	PBMcs			
(1)	×	SPG4 (1)	C75insA	×	×
(2)	×	SPG4 (2)	C1215-1219DTATAA9	×	×
(3)	×	SPG4 (3)	C1215-1219DTATAA9	×	×
(4)		SPG4 (4)	C910-914DCCTACTinTAG		×
(5)		SPG4 (5)	C1536G-C		×
(6)		SPG4 (6)	c.1280T>C (p.Phe427Ser)	×	
(7)		SPG4 (7)	c.1130G>A (p.Gly377Glu)	×	
(8)		SPG4 (8)	c.1636G>C(p.Gly564Arg)	×	
(9)		SPG7 (1)	c.1807G>A (p.Ala603Thr); c.862-3C>T [r?; splicing]		×
		SPG7 (2)	c.273_274delCT/p. Trp92Alafs*; c.679C>T/p. Arg227*		×
		SPG7 (3)	c.1529C>T (p.Ala510Val); c.1053delC		×
		SPG11 (1)	c.4307_4308delAA; c.662G>A (p.Trp221*)		×
		SPG11 (2)	c.4307_4308delAA; c.4307_4308delAA		×
		SPG30 (1)	c.32G>G (p.R11P)		×
		SPG30 (2)	c.1038G>C (p.R346S)		×
		SPG30 (3)	c.761G>A (p.R254Q)		×
		SPG3a (1)	c.1688insA		×
		SPG3a (2)	c.1308T>A (p.N436K)		×

Abbreviations: HD, healthy donor; HSP, hereditary spastic paraplegia; LCLs, lymphoblastoid cells; PBMcs, peripheral blood mononuclear cells.

Immunofluorescence (IF) and automated image analysis

Cells were seeded onto poly-L-lysine coated coverslips as in Prodosmo et al. [17], fixed in 2% formaldehyde, permeabilized in 0.25% Triton X-100 in phosphate-buffered saline (PBS) for 10 min, and then blocked in 5% bovine serum albumin in PBS before the primary Ab was applied. The following Abs were employed: anti- α -tubulin-FITC #F2168, anti- β -tubulin-cy3 #C4585, anti-acetyl- α -tubulin #T7451 (Sigma-Aldrich). Secondary mouse TRITC Abs #A11005 (Alexa-fluor, Life Technologies) were used. DNA was marked with Hoechst (Sigma-Aldrich). Cells were examined under an inverted microscope (Eclipse Ti, Nikon) using a Clara camera (Andor technology). Images for each sample were taken in parallel using an identical microscope by NIS-Elements H.C. 5.11 using the JOBS module for automated acquisitions. Analysis was performed using customized image analysis pipelines in CellProfiler. Briefly, the intensity of β -tubulin is calculated as the average pixel intensity within a selected region of interest (ROI), the 'form factor' is calculated as $4\pi \times \text{area}/\text{perimeter}^2$ of a ROI set to the tubulin staining, and

the 'dncn' is calculated as the length of the line segment joining two points (i.e., the nucleus and cell centroids, set to the Hoechst and tubulin ROIs respectively).

Flow cytometry analysis

To analyse the cell-cycle phase distribution, LCLs were collected by centrifugation, washed with PBS and fixed with 50% methanol overnight at 4°C. Cell-cycle phase distribution was analysed after incubation for 30 min in the dark with propidium iodide (0.03 mg/ml) and RNase A (0.2 mg/ml) using a flow cytometer Epics XL apparatus (Beckman Coulter). Cell aggregates were gated out on a bi-parametric graph FL-3 in ratio as described by Ferrara et al. [19]. Cell samples were analysed in a Coulter Epics XL cytofluorometer (Beckman Coulter) equipped with EXPO 32 ADC software. At least 10,000 cells per sample were acquired. The percentage of cells in the different phases of the cell cycle was calculated using Flowing Software 2.5. For the analysis of the forward scatter (FSC) and side scatter (SSC), LCLs were collected and freshly analysed without fixation.

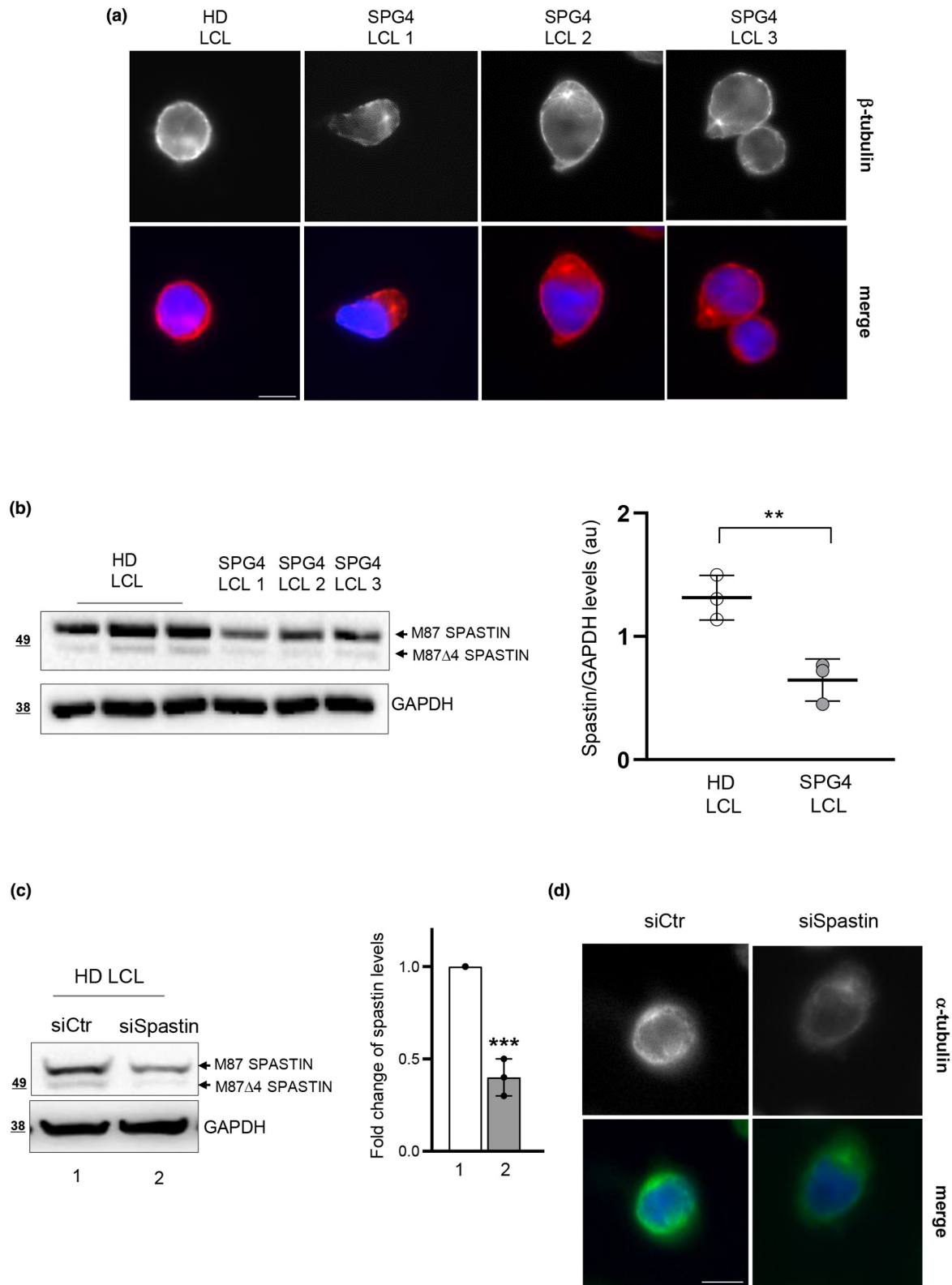
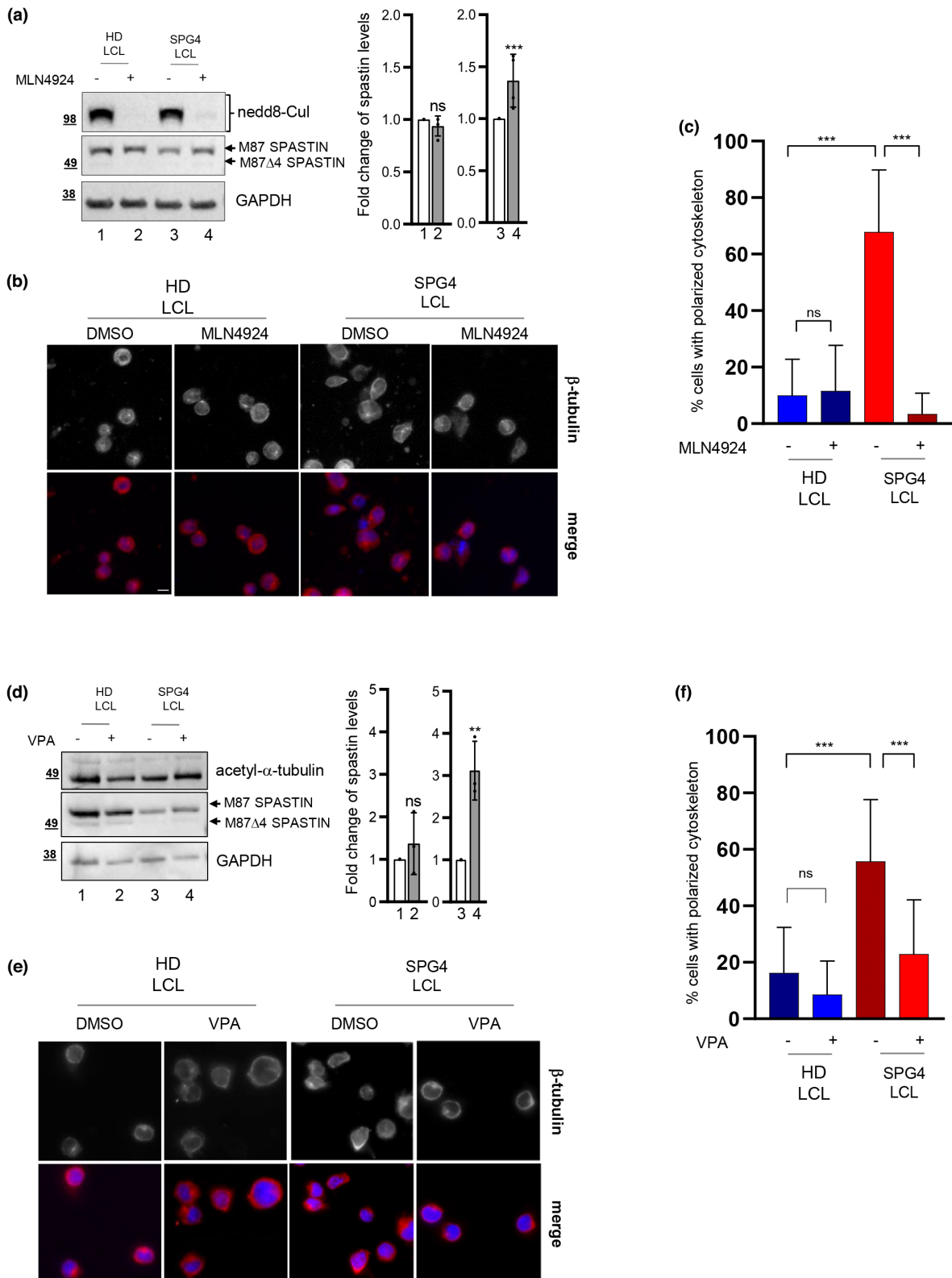


FIGURE 1 MT cytoskeleton organization in LCLs. (a) The indicated cells were analysed by IF. Cells were stained with anti- β -tubulin Ab and counterstained with Hoechst for nucleus labelling. Representative images are shown. (b) The indicated LCLs were analysed by WB. Unless otherwise indicated, here and in all the figures, a representative WB of three independent experiments is shown and molecular weight markers are reported in kilodaltons. The quantification of the WB is shown in the right panel; the intensity of the spastin bands was quantified, normalized and reported as mean \pm standard deviation (SD) for the indicated cells. $^{**}p < 0.001$, *t* test. au, arbitrary units. (c), (d) HD LCLs were transfected using 40nM spastin-specific (siSpastin) or negative control (siCtr) stealth siRNAs and analysed by WB and IF 48h post transfection. (c) Representative WB showing the decrease of spastin protein levels in the left panel and quantification of WB results as mean \pm SD from three independent experiments in the right panel. $^{***}p < 0.0001$; *t* test. (d) Cells were stained with anti- α -tubulin Ab and counterstained with Hoechst for nucleus labelling; representative images are shown. Scale bars 10 μ M.

Statistical analysis

Unless otherwise indicated, data from at least three experiments were statistically analysed using GraphPad Prism software 6. Normal distribution of parameters was assessed by using

the Shapiro-Wilk test. For measurements of continuous variables the unpaired Student's *t* test or ordinary one-way ANOVA Bonferroni's multiple comparison tests were used. When samples were not normally distributed Mann-Whitney tests were used instead of the unpaired Student's *t* test. Pearson correlation was



used to measure relationships between pairs of continuous variables. Statistical significance was set at $p < 0.01$ and was reported by asterisks according to the following scheme: *** $p < 0.0001$, ** $p < 0.001$.

RESULTS

Spastin haploinsufficient SPG4 LCLs show a polarized MT cytoskeleton organization

In the process of studying spastin-enhancing treatments, it was observed that LCLs from patients carrying heterozygous haploinsufficient SPG4 truncating mutations show a polarized MT cytoskeleton organization compared to LCLs derived from HDs or patients with other genetic disorders unrelated to SPG4, such as AT or WS (Figures 1a–c, S1a–c and Table 1). Anti- β -tubulin or anti- α -tubulin or anti-acetyl- α -tubulin Abs were used to mark MTs in combination with Hoechst to counterstain nuclei (Figures 1 and S1). Differently from HD, AT and WS LCLs that are rounded with a central nucleus surrounded by a thin layer of MT cytoskeleton, SPG4 LCLs appear with an eccentric nucleus and polarized MT cytoskeleton organization (Figures 1a and S1a–c).

To evaluate whether this SPG4 LCL phenotype might be induced by spastin level reduction, spastin protein levels were first verified in our SPG4 LCLs. According to the type of SPG4 truncating mutations (Table 1) and literature evidence [20, 21], WB analyses showed a significant reduction of approximately 50% of spastin protein levels in the SPG4 LCLs compared to HD LCLs, whilst, as expected, the spastin truncated forms and M1 isoforms were undetectable (Figures 1b and S1d,e). Next, a reduction of spastin protein levels was induced like those of haploinsufficient SPG4-HSP patients' cells in the HD LCLs. As shown in Figure 1c,d, it was observed that a reduction of spastin levels obtained by RNAi induces an MT cytoskeleton organization similar to those of SPG4 LCLs, supporting the hypothesis that the MT cytoskeleton is affected by reduced spastin levels. Comparable results were obtained by treating HD LCLs with the ATP-competitive inhibitor spastazoline that blocks the catalytic activity of spastin [22] (Figure S1f), suggesting that the polarized MT cytoskeleton organization can also be induced by spastin inactivation.

Spastin-enhancing drugs rescue the MT cytoskeleton organization in SPG4 LCLs

Since it has been demonstrated previously that MLN4924 treatment can increase spastin protein levels in SPG4 LCLs [13], it was evaluated whether MLN4924 treatment is able to rescue the MT cytoskeleton organization in SPG4 LCLs. Thus, SPG4 LCLs were treated with MLN4924 or its solvent, DMSO as in Sardina et al. [13], and analysed by WB to verify the efficacy of the treatment in restoring spastin protein levels and by IF to evaluate the MT cytoskeleton organization. It was observed that the increase of spastin levels associates with a significant rescue of MT cytoskeleton organization in SPG4 LCLs (Figure 2a–c).

To exclude cell-cycle-dependent effects of MLN4924 treatment on MT cytoskeleton organization, flow cytometry analysis was performed using propidium iodide DNA staining. The analyses did not reveal any change in the cell-cycle distribution of SPG4 and HD LCLs (Figure S2a,b).

Recently, VPA has been shown to restore spastin protein levels in the cortical neurons of a mouse model of autosomal recessive spinocerebellar ataxia 20 (SCAR20), characterized by spastin destabilization [23]. Thus, as a further approach, VPA was employed. First, it was assessed whether VPA treatment restores spastin levels also in SPG4 LCLs and then its effects on the MT cytoskeleton were analysed. As shown in Figure 2d–f, VPA increases spastin levels and rescues MT cytoskeleton organization in SPG4 LCLs.

Taken together, these results indicate that the polarized MT cytoskeleton organization of SPG4 LCLs is reversible and can be rescued by restoring spastin levels.

SPG4 and spastin-deficient LCLs show an increase of the distance between cell and nucleus centroids

Based on the above observations, the possibility of quantifying the morphological features of SPG4 LCLs detected by MT staining was evaluated. This was begun by building a customized pipeline for automated image analysis using the open-source software CellProfiler [24]. Using this pipeline, the SPG4 and HD LCLs were analysed by measuring different parameters, that is, the intensity

FIGURE 2 Spastin-enhancing treatments in LCLs. (a)–(c) The indicated cells were treated with MLN4924 or its solvent DMSO and analysed by WB or IF 16 h post treatment. (a) Representative WB with indicated Abs; cullin deneddylation is shown as MLN4924 positive control. The intensity of the spastin bands was quantified, normalized and reported relative to solvent treatment as mean \pm SD from four independent experiments in the right panels. *** $p < 0.0001$; ns, not statistically significant; t test. (b) Representative images of indicated cells stained as in Figure 1(a). (c) Histogram showing the percentage of cells characterized by a polarized organization of MT cytoskeleton is reported as mean \pm SD from three independent experiments, in which >200 cells were manually analysed (cells showing an eccentric nucleus and an elongated tubulin staining/total cells). *** $p < 0.0001$; one-way ANOVA Bonferroni's multiple comparison test. (d)–(f) Indicated cells were treated with VPA or its solvent DMSO and analysed as in (a)–(c) 24 h post treatment. (d) Representative WB with indicated Abs; an increase of acetyl- α -tubulin is shown as VPA positive control. (e) Representative images of indicated cells stained as in (a). (f) Histogram obtained as in (d). *** $p < 0.0001$; one-way ANOVA Bonferroni's multiple comparison test. Scale bars 10 μ m. Data from SPG4 LCL1 and HD LCL1 are shown. Similar data were obtained by analysing SPG4 LCL2 and HD LCL2.

of β -tubulin staining, the 'form factor' and the distance between nucleus and cell centroid (dcnc) for each single cell under consideration. The measurements of the first two parameters did not distinguish the MT cytoskeleton organization of SPG4 LCLs compared to controls. The intensity of the β -tubulin staining increased in SPG4 LCLs 1 and 3 and decreased in SPG4 LCL 2 compared to control HD LCLs; similar data were also obtained by measuring the intensity of the acetyl- α -tubulin staining (Figure S3a,b). The 'form factor', a measure that reflects the shape of objects, did not detect significant changes between HD and SPG4 LCLs (Figure 3a), whereas a significant increase of the dcnc was sufficient to distinguish the SPG4 LCL MT organization compared to HD controls (Figure 3b,c). Next, the pipeline was used to automatically analyse the images relative to the experiments reported in Figures 1e and S1e, showing that a significant increase of the dcnc parameter characterizes the MT cytoskeleton organization induced by the reduction of spastin protein levels or the inhibition of its activity (Figure 3d,e). This suggests that an automated cellular imaging dcnc-based method might be used as a test to specifically recognize SPG4 LCLs and to detect spastin-dependent effects in the organization of the LCL MT cytoskeleton.

The dcnc-based method is able to recognize the polarized MT cytoskeleton organization in PBMCs isolated from SPG4 -HSP patients

After having verified that freshly isolated SPG4 PBMCs show an MT cytoskeleton organization like that of SPG4 LCLs (Figure S4a), whether the dcnc-based method can be used to discriminate the MT cytoskeleton organization of PBMCs isolated from SPG4-HSP patients and HDs was investigated. PBMCs from five patients and four HDs (Table 1) were isolated and analysed. On performing grouped (Figure 4a) and individual evaluations (Figure S4b), SPG4 PBMCs showed a statistically significant increase of the dcnc parameter compared to HD PBMCs. Comparable results were obtained by analysing PBMCs isolated from whole blood maintained at room temperature for 48 or 72h and containing EDTA as anticoagulant, or PBMCs frozen in DMSO and then thawed, testing the cells under different experimental conditions (Figure S4c). These findings indicate that the polarized MT cytoskeleton organization is not modified by Epstein-Barr virus mediated immortalization or cell manipulation. Of relevance, these characteristics allow this method to be used as a simple and rapid test to analyse PBMCs, obviating the need for laborious and time-consuming stabilization of LCLs.

To evaluate the specificity of the dcnc-based method, PBMCs isolated from patients carrying different SPG types of HSP (Table 1) due to mutations in proteins affecting MT dynamics, such as the kinesin motor protein KIF1A (SPG30 [25]) and the spastin interactor Atlastin-1 (SPG3a [26]), or in proteins affecting MT-independent processes, such as the mitochondrial metalloprotease paraplegin (SPG7 [27]) or the vesicle trafficking associated protein spatacsin (SPG11

[28]) were analysed. On using the dcnc-based method, the PBMCs carrying these SPG-HSP subtypes do not show any increase of dcnc compared to HD PBMCs and are significantly different from SPG4 PBMCs (Figure 4b).

The dcnc-based method senses the effects of a spastin-enhancing drug in PBMCs

To assess whether the dcnc-based method can detect the effects of spastin-enhancing treatments in PBMCs, SPG4 and HD PBMCs were treated with MLN4924 or its solvent, DMSO. First, it was verified that, as has been observed for the SPG4 LCLs, the MLN4924 treatment was able to increase spastin levels also in SPG4 PBMCs (Figure 5a). Next, the MT cytoskeleton organization of the treated cells was analysed, showing a significant reduction of the dcnc parameter in MLN4924 treated cells compared to solvent-treated control (Figure 5b), suggesting that this method might be used as a fast readout parameter for spastin recovery in non-neuronal cells.

DISCUSSION

The identification of non-invasive biomarkers, such as blood cell imaging-based markers, is an emerging challenge for neurodegenerative disorders (NDs). A polarized MT cytoskeleton organization in the blood mononuclear cells isolated from patients affected by SPG4-HSP was observed that led us to the development of an automated dcnc-based method, which can detect and quantify changes in the MT cytoskeleton organization of PBMCs from patient samples. Interestingly, the polarized MT organization is not permanent and can be reverted by restoring para-physiological spastin levels in SPG4 cells or induced in HD LCLs by lowering the levels of spastin or inhibiting its activity. These observations indicate that the polarized MT cytoskeleton organization is a phenotype strongly dependent on spastin dosage and functionality. Amongst the imaging parameters that were sought to describe this phenotype, the focus was mainly on those relative to cell morphology, such as the 'form factor' and the dcnc. It was found that the dcnc-based method senses spastin level changes and distinguishes LCLs and PBMCs carrying SPG4 truncating mutations from HD controls. In addition, dcnc senses MT organization changes induced by spastin inactivation by an ATP-competitive inhibitor. Thus, to begin evaluating whether the dcnc-based method can also discriminate SPG4 missense mutations, LCLs were analysed from three patients carrying three different missense mutations in the catalytic domain (Table 1,5). Consistent with the effect of the spastin inhibitor, dcnc was able to discriminate the missense SPG4-carrying LCLs from those of the HDs (Figure S5). By analysing LCLs from patients carrying other types of HSP mutations, such as those in proteins involved in MT-dependent or MT-independent functions, evidence was

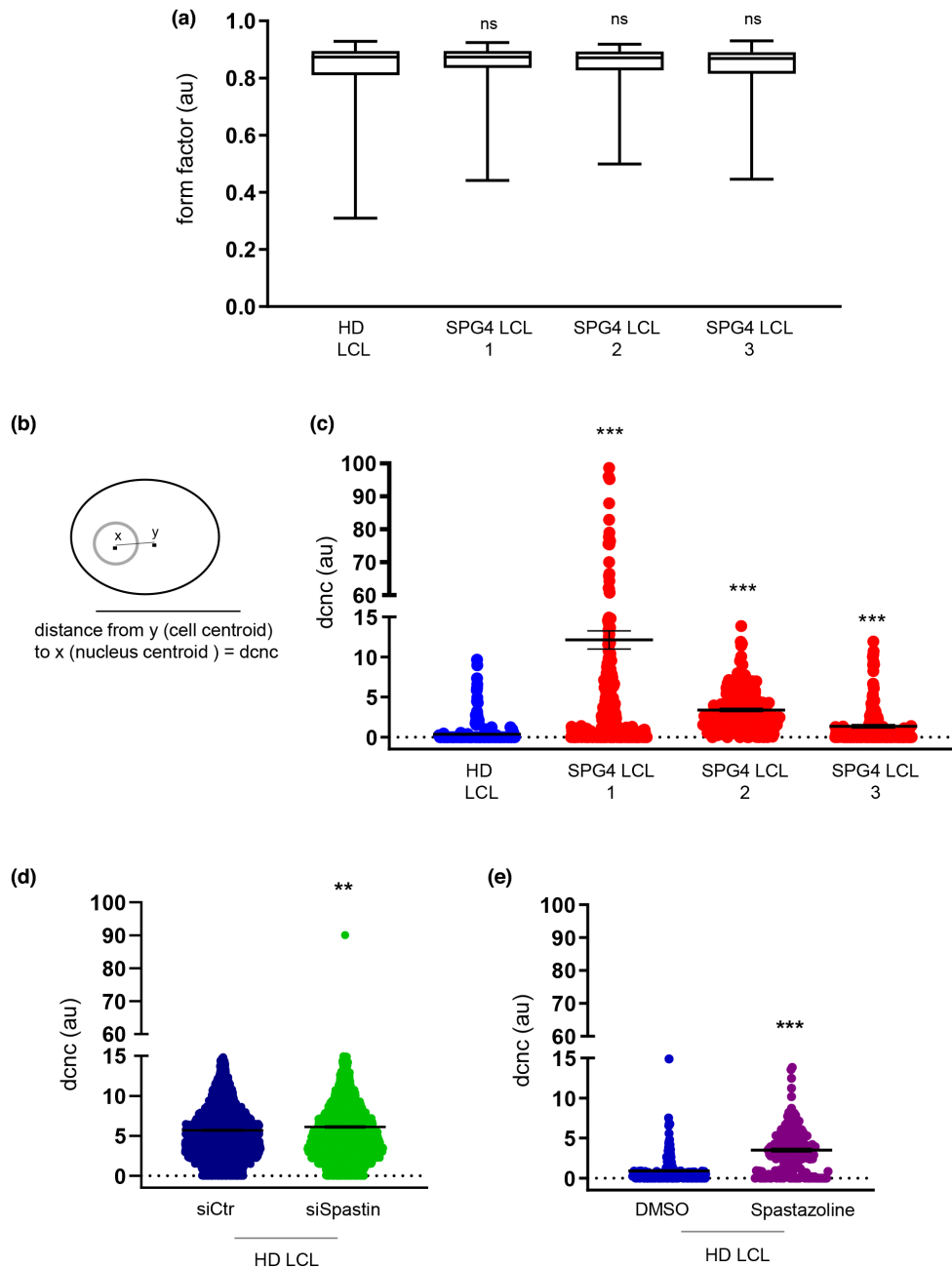


FIGURE 3 *SPG4* and spastin-deficient LCLs show an increase of the dncn compared to control LCLs. (a)–(c) The indicated cells were stained as in Figure 1(a); automated image analyses were performed by using a customized CellProfiler pipeline and different parameters were calculated for each cell; at least 100 cells were analysed per condition, in three independent experiments. (a) Box plots to compare the ‘form factor’ parameter in *SPG4* and HD LCLs are reported; the Mann–Whitney test relative to control is not statistically significant. (b) Schematic representation of the dncn parameter. (c) Dot plots to compare the dncn in *SPG4* and HD LCLs are reported. Each dot represents a single cell; the horizontal black lines indicate the mean \pm standard error of the mean (SEM) and the Mann–Whitney test is relative to HD LCLs. *** $p < 0.0001$. (d), (e) The images relative to the experiments shown in the Figure 1(e) and Figure S1(e) were automatically analysed and reported as in (c). ** $p < 0.001$, *** $p < 0.0001$; t test.

obtained supporting the specificity of the dncn-based method for *SPG4*-HSP. However, it cannot be excluded that an MT cytoskeleton organization resembling those of *SPG4* cells might be present in other MT-associated HSP subtypes that we have not yet analysed (e.g., *SPG31*, *SPG58*, *SPG72*).

Altogether, these results support the dncn-based method as a suitable potential biomarker responding to changes in spastin levels and function in non-neuronal cells. A large-scale study will be necessary to define whether the dncn-based method could be a biomarker for *SPG4*-HSP alone or in combination with other parameters.

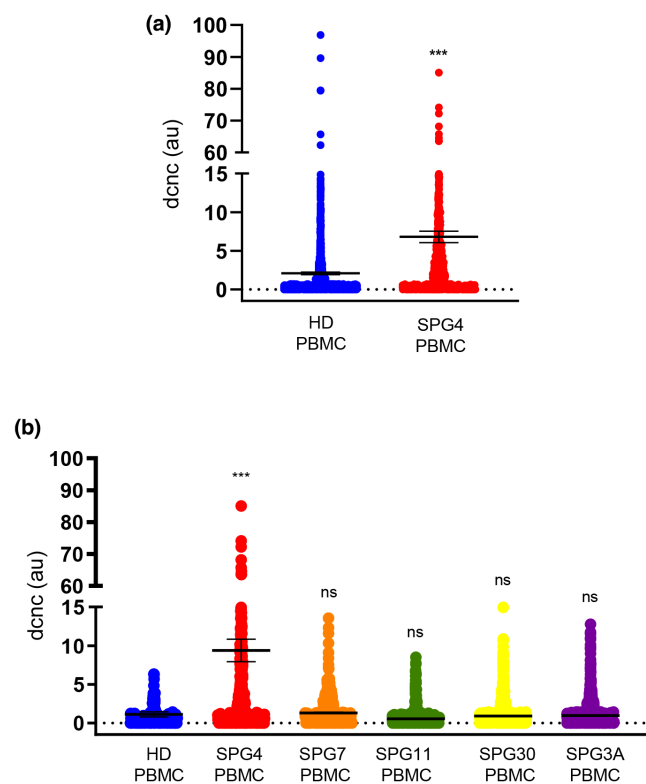


FIGURE 4 Dcnc analyses in PBMCs from different HSP patients. (a) The indicated cells were analysed in duplicate after staining as in Figure 1(a), using a customized CellProfiler pipeline. Grouped analysis of the dncn in PBMCs from *SPG4*-HSP patients compared to PBMCs from HDs is shown. The horizontal black lines indicate the mean \pm SEM. *** $p < 0.0001$, *t* test. (b) Cells were stained and automatically analysed as in (a). Grouped analysis of the dncn in PBMCs from indicated HSP patients compared to HD. The horizontal black lines indicate the mean \pm SEM; *** $p < 0.0001$, one-way ANOVA Bonferroni's multiple comparison test.

The establishment of a multiparametric readout could implement our analysis. The correlation between dncn/form factor, dncn/tubulin intensity and form factor/tubulin intensity was analysed. As shown in Figure S6a, there is no significant correlation between the indicated parameters. However, it would be interesting to perform future investigations aimed at combining dncn with parameters relative to other organelles known to be affected by spastin dysfunction (e.g., size/distribution/number of lipid droplets, peroxisomes, lysosomes, mitochondria).

It is known that MT length and density play an important role in MT cytoskeleton organization and recent evidence supports spastin as a key enzyme in shaping MT networks by promoting both MT disassembly and growth [29, 30]. It has been observed that neural cells and fibroblasts lacking spastin activity develop long MT fragments [15] and a polarized morphology, showing long protrusions filled with a linear array of acetylated MTs [31], a phenotype reminiscent of the polarized organization of the MT cytoskeleton observed in spastin-deficient LCLs and PBMCs. The focus of our

attention is *SPG4* PBMCs because they are easily accessible cells, opening the possibility of identifying a first rapid outcome measure for spastin recovery in non-neuronal cells. It will be relevant to verify whether this phenotype is also present in patient neuronal cells.

The local concentration and the rate of the spastin severing activity, the MT dynamic properties in combination with MT-associated proteins, and the fate of the severed MT tips might affect the spatial organization of the MT networks with consequence on the selective transport of the organelles and cargos that are needed for proper cellular activity. Thus, it will be important to evaluate whether the MT organization observed in the *SPG4* PBMCs leads to defects in MT-dependent functions, such as intracellular trafficking and directional cell migration. By affecting the cytoskeleton organization, spastin might also influence the MT array maintenance and orientation during neural development and tissue morphogenesis, whose implications in HSP pathogenesis still need to be explored.

Drugs acting on MT dynamics have been shown to rescue some *SPG4*-HSP defects in several models [32]. Recently, the effects of noscapine have been assessed in *SPG4*-HSP patient-derived fibroblasts by using cell morphology profiling [33]. An evaluation of the effects of MT drugs (such as noscapine, vinblastine, nocodazole and epothilone B) on the MT cytoskeleton organization of *SPG4* LCLs and PBMCs could now be performed by using the dncn-based method.

To date, there is no unambiguous genotype–phenotype correlation for *SPG4*-HSP patients [3]. Thus, from a clinical point of view, it will be interesting to extend our analyses to a large cohort of *SPG4*-HSP patients, with different mutations and disease severity, and to investigate the relationship between the observed phenotype and the clinical characteristics by performing cross-sectional and longitudinal studies.

Altered MT dynamics is a common feature of sporadic NDs, such as Alzheimer's disease, Amyotrophic Lateral Sclerosis, Parkinson's disease and Huntington's disease [34, 35]. Our *SPG4*-HSP studies might represent a model by tracing the way for identifying useful biomarkers for sporadic NDs.

Additionally, the MT cytoskeleton organization of *SPG4* LCLs is distinguishable also by flow cytometry analysis. As shown in Figure S6b,c, a reproducible and consistent slight increase of the FSC and a statistically significant increase of the SSC in *SPG4* LCLs were observed compared with HD LCLs. An increase of these two parameters (indicating the size of the cells and the complexity/granularity of the cells, respectively) may be in agreement with the phenotypes observed by IF, but deserves further investigations.

Overall, our findings support the MT cytoskeleton organization of PBMCs as an easily accessible potential biomarker for *SPG4*-HSP and reveal new non-invasive tools for *SPG4*-HSP diagnosis, monitoring, prognosis and predictivity.

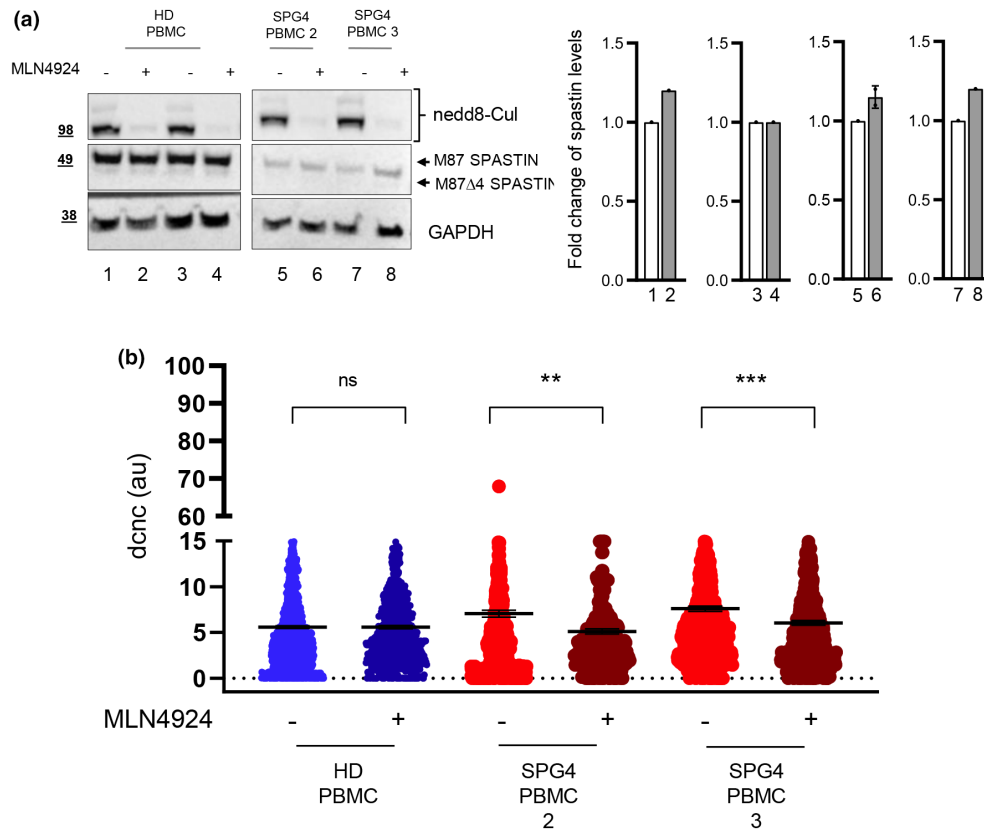


FIGURE 5 Effects of a spastin-enhancing drug in *SPG4* PBMCs. (a), (b) The indicated cells were treated as in Figure 2(a) and analysed by WB and IF. (a) Representative WB and its quantification. Cullin deneddylation is shown as MLN4924 positive control. Samples were run on the same gel and processed on the same filter. The intensity of the spastin bands was quantified, normalized and reported relative to solvent treatment as mean \pm SD from two independent experiments in the right panel. (b) Automated image analysis was performed as in Figure 4(a) and dot blot of the indicated parameter is shown; ** $p < 0.01$; *** $p < 0.0001$; one-way ANOVA Bonferroni's multiple comparison test.

ACKNOWLEDGEMENTS

The authors thank the patients and families for their collaboration, Dr Giulia Federici for WS LCL management, Dr Valerio Licursi for critical discussion about statistical analyses and Dr Serena Mero for *SPG7*, *SPG11*, *SPG30* and *SPG3a* PBMC management in FMS laboratories. Open Access Funding provided by Consiglio Nazionale delle Ricerche within the CRUI-CARE Agreement.

FUNDING INFORMATION

This study was supported by grants from AFM-Telethon #22157, Telethon #GGP20040, the UK-HSP support group, Regione LAZIO 'Progetti di Gruppi di Ricerca 2020' project ID A0375-2020-36597, to CR; AFM-Telethon #23786, Euro HSP and A.I.V.I.P.S. to FS; the Italian Ministry of Health (Ricerca Finalizzata RF-2016-02361610 and Ricerca Corrente 5x1000) to FMS. The funders had no role in study design, data collection and analysis, decision to publish, or preparation of the manuscript.

CONFLICT OF INTEREST STATEMENT

All authors declare that they have no conflicts of interest.

DATA AVAILABILITY STATEMENT

The authors confirm that the data supporting the findings of this study are available within the article and its supplementary materials. Row data will be available on reasonable request.

ORCID

Francesca Sardina  <https://orcid.org/0000-0001-6474-2079>

REFERENCES

- Lallemant-Dudek P, Darios F, Durr A. Recent advances in understanding hereditary spastic paraplegias and emerging therapies. *Fac Rev.* 2021;10(10):27. doi:10.12703/r/10-27
- Fink JK. Hereditary spastic paraplegia: clinico-pathologic features and emerging molecular mechanisms. *Acta Neuropathol.* 2013 Sep;126(3):307-328. doi:10.1007/s00401-013-1115-8
- Parodi L, Fenu S, Barbier M, et al. Spastic paraplegia due to SPAST mutations is modified by the underlying mutation and sex. *Brain.* 2018;141(12):3331-3342. doi:10.1093/brain/awy285
- Claudiani P, Riano E, Errico A, Andolfi G, Rugarli EI. Spastin sub-cellular localization is regulated through usage of different translation start sites and active export from the nucleus. *Exp Cell Res.* 2005;309(2):358-369. doi:10.1016/j.yexcr.2005.06.009

5. Rossi S, Rubegni A, Riso V, et al. Clinical-genetic features influencing disability in spastic paraplegia type 4: a cross-sectional study by the Italian DAISY network. *Neural Genet.* 2022;8(2):e664. doi:10.1212/NXG.0000000000000664
6. Hedera P. Hereditary Spastic Paraplegia Overview. In: Adam MP, Ardinger HH, Pagon RA, et al., eds. *GeneReviews® [Internet]*. University of Washington, Seattle; 2000:1993-2022.
7. Parodi L, Rydning SL, Tallaksen C, Durr A. Spastic Paraplegia 4. In: Adam MP, Ardinger HH, Pagon RA, et al., eds. *GeneReviews® [Internet]*. University of Washington, Seattle; 2003:1993-2022.
8. Gaetani L, Blennow K, Calabresi P, Di Filippo M, Parnetti L, Zetterberg H. Neurofilament light chain as a biomarker in neurological disorders. *J Neurol Neurosurg Psychiatry.* 2019;90(8):870-881. doi:10.1136/jnnp-2018-320106
9. Kessler C, Serna-Higuaita LM, Rattay TW, et al. Neurofilament light chain is a cerebrospinal fluid biomarker in hereditary spastic paraplegia. *Ann Clin Transl Neurol.* 2021;8(5):1122-1131. doi:10.1002/acn3.51358
10. Kessler C, Serna-Higuaita LM, Wilke C, et al. Characteristics of serum neurofilament light chain as a biomarker in hereditary spastic paraplegia type 4. *Ann Clin Transl Neurol.* 2022;9(3):326-338. doi:10.1002/acn3.51518
11. Rattay TW, Völker M, Rautenberg M, et al. The prodromal phase of hereditary spastic paraplegia type 4: the preSPG4 cohort study. *Brain.* 2022;26:awac155. doi:10.1093/brain/awac155
12. Havlicek S, Kohl Z, Mishra HK, et al. Gene dosage-dependent rescue of HSP neurite defects in SPG4 patients' neurons. *Hum Mol Genet.* 2014;23(10):2527-2541. doi:10.1093/hmg/ddt644
13. Sardina F, Pisciotanni A, Ferrara M, et al. Spastin recovery in hereditary spastic paraplegia by preventing neddylation-dependent degradation. *Life Sci Alliance.* 2020;3(12):e202000799. doi:10.26508/lsa.202000799
14. Vajente N, Norante R, Redolfi N, Daga A, Pizzo P, Pendin D. Microtubules stabilization by mutant spastin affects ER morphology and Ca²⁺ handling. *Front Physiol.* 2019;20(10):1544. doi:10.3389/fphys.2019.01544
15. Lopes AT, Hausrat TJ, Heisler FF, et al. Spastin depletion increases tubulin polyglutamylation and impairs kinesin-mediated neuronal transport, leading to working and associative memory deficits. *PLoS Biol.* 2020;18(8):e3000820. doi:10.1371/journal.pbio.3000820
16. Liu Q, Zhang G, Ji Z, Lin H. Molecular and cellular mechanisms of spastin in neural development and disease (review). *Int J Mol Med.* 2021;48(6):218. doi:10.3892/ijmm.2021.5051
17. Prodosmo A, De Amicis A, Nisticò C, et al. p53 centrosomal localization diagnoses ataxia-telangiectasia homozygotes and heterozygotes. *J Clin Invest.* 2013;123(3):1335-1342. doi:10.1172/JCI67289
18. Pisciotanni A, Biancolillo L, Ferrara M, et al. HIPK2 phosphorylates the microtubule-severing enzyme spastin at S268 for abscission. *Cell.* 2019;8(7):684. doi:10.3390/cells8070684
19. Ferrara M, Sessa G, Fiore M, et al. Small molecules targeted to the microtubule-Hec1 interaction inhibit cancer cell growth through microtubule stabilization. *Oncogene.* 2018;37(2):231-240. doi:10.1038/ncr.2017.320
20. Charvin D, Cifuentes-Diaz C, Fonknechten N, et al. Mutations of SPG4 are responsible for a loss of function of spastin, an abundant neuronal protein localized in the nucleus. *Hum Mol Genet.* 2003;12(1):71-78. doi:10.1093/hmg/ddg004
21. Nan H, Chu M, Liu L, Xie K, Wu L. A novel truncating variant of SPAST associated with hereditary spastic paraplegia indicates a haploinsufficiency pathogenic mechanism. *Front Neurol.* 2022;14(13):1005544. doi:10.3389/fneur.2022.1005544
22. Cupido T, Pisa R, Kelley ME, Kapoor TM. Designing a chemical inhibitor for the AAA protein spastin using active site mutations. *Nat Chem Biol.* 2019;15(5):444-452. doi:10.1038/s41589-019-0225-6
23. Zhang H, Hong Y, Yang W, et al. SNX14 deficiency-induced defective axonal mitochondrial transport in Purkinje cells underlies cerebellar ataxia and can be reversed by valproate. *Natl Sci Rev.* 2021;8(7):nwab024. doi:10.1093/nsr/nwab024
24. Carpenter AE, Jones TR, Lamprecht MR, et al. CellProfiler: image analysis software for identifying and quantifying cell phenotypes. *Genome Biol.* 2006;7(10):R100. doi:10.1186/gb-2006-7-10-r100
25. Pennings M, Schouten MI, van Gaalen J, et al. KIF1A variants are a frequent cause of autosomal dominant hereditary spastic paraplegia. *Eur J Hum Genet.* 2020;28(1):40-49. doi:10.1038/s41431-019-0497-z
26. Park SH, Zhu PP, Parker RL, Blackstone C. Hereditary spastic paraplegia proteins REEP1, spastin, and atlastin-1 coordinate microtubule interactions with the tubular ER network. *J Clin Invest.* 2010;120(4):1097-1110. doi:10.1172/JCI40979
27. Casari G, Marconi R. Spastic Paraplegia 7. In: Adam MP, Ardinger HH, Pagon RA, et al., eds. *GeneReviews® [Internet]*. University of Washington, Seattle; 2006, 1993-2022.
28. Stevanin G. Spastic Paraplegia 11. In: Adam MP, Ardinger HH, Pagon RA, et al., eds. *GeneReviews® [Internet]*. University of Washington, Seattle; 2008, 1993-2022.
29. Kuo YW, Cutting HJ. Amplifying, and aligning microtubules with severing enzymes. *Trends Cell Biol.* 2021;31(1):50-61. doi:10.1016/j.tcb.2020.10.004
30. Yogev S, Cooper R, Fetter R, Horowitz M, Shen K. Microtubule organization determines axonal transport dynamics. *Neuron.* 2016;92(2):449-460. doi:10.1016/j.neuron.2016.09.036
31. Connell JW, Allison RJ, Rodger CE, Pearson G, Zlamalova E, Reid E. ESCRT-III-associated proteins and spastin inhibit protrusion-dependent polarised membrane traffic. *Cell Mol Life Sci.* 2020;77(13):2641-2658. doi:10.1007/s00018-019-03313-z
32. Boiarska Z, Passarella D. Microtubule-targeting agents and neurodegeneration. *Drug Discov Today.* 2021;26(2):604-615. doi:10.1016/j.drudis.2020.11.033
33. Wali G, Berkovsky S, Whiten DR, Mackay-Sim A, Sue CM. Single cell morphology distinguishes genotype and drug effect in hereditary spastic paraplegia. *Sci Rep.* 2021;11(1):16635. doi:10.1038/s41598-021-95995-4
34. Brandt R, Bakota L. Microtubule dynamics and the neurodegenerative triad of Alzheimer's disease: the hidden connection. *J Neurochem.* 2017;143(4):409-417. doi:10.1111/jnc.14011
35. Pellegrini L, Wetzel A, Grannó S, Heaton G, Harvey K. Back to the tubule: microtubule dynamics in Parkinson's disease. *Cell Mol Life Sci.* 2017;74(3):409-434. doi:10.1007/s00018-016-2351-6

SUPPORTING INFORMATION

Additional supporting information can be found online in the Supporting Information section at the end of this article.

How to cite this article: Sardina F, Valente D, Fattorini G, et al. New cellular imaging-based method to distinguish the SPG4 subtype of hereditary spastic paraplegia. *Eur J Neurol.* 2023;30:1734-1744. doi:10.1111/ene.15756